RESISTANCE HEATING

INTRODUCTION

Resistance heating in general is an unwanted side-effect in electrical engineering. As resistive losses cost energy and as dissipated energy may result in unacceptably high levels of device temperature, considerable efforts are put into transforming energy as efficiently as possible. In case excessive heating cannot be avoided, thermal energy needs to be withdrawn from the heat generating devices using heat sinks. Heat sinks are often more expensive and much larger in size than the overheating devices themselves (e.g. transistors). Aiming at small-size electronic equipment, heat dissipation therefore needs to be kept to a minimum.

On the other hand, there are also devices that need to be heated for proper operation. In this latter context resistive heating has the advantage of being amenable to electronic control. Further, as temperature can easily be measured using temperature sensors, the temperature of a heated component can be kept constant using closed-loop control. Compared to combustion, resistive heating is also less dangerous. To maintain combustion, a minimum temperature is required which in general is well above the temperature required for optimum device operation. In case of an accident, high combustion temperatures may also prove to be harmful. In the case of resistive heating, on the other hand, the maximum temperature inside a heating resistor need not be much higher than the desired surface temperature. In those cases, however, in which large amounts of heat are to be generated it has to be kept in mind that chemical energy presently can only be transformed into electrical energy with an efficiency of about 40%. Combustion heating, therefore may prove to be overall more advantageous when large quantities of heat have to be generated.

In this article we focus on resistance heating in miniaturized electronic devices, i.e. thermal sensors and thermal actuators. Such devices are transducers of energy, which involve thermal energy conversion on an intermediate stage. In such devices heat dissipation is not an unwanted byproduct of the energy conversion process but rather constitutes the central mechanism that underlies device operation. Some industrially important kinds of such sensor and actuator devices are explained in more detail below.

THERMAL SENSORS AND ACTUATORS

Sensors are transducers that convert nonelectrical input signals into electrical output signals. The interest in electricity relies on the fact that electrical output signals lend themselves to effective amplification, processing and communication (1). Sensors can broadly be classified into five major classes according to the input energy forms of the signals to be detected:

Signal domain	**Transduction effect**
mechanical	piezoresistive effect
thermal	pn-diode voltage, thermo-electric voltage
chemical	chemically induced field effect
magnetic	Hall effect
electro-magnetic radiation	photo-conductive effect, pn-photo-effect.

As indicated in the list above, semiconductors - and crystalline silicon in general - offer a number of solid-state effects that allow the above five kinds of non-electrical input signals to be directly converted into electrical output signals (2).

In the case of mechanical input signals it is further relevant to note that silicon can be shaped into miniaturized mechanical structures that can be measurably deformed under the action of mechanical input signals such as pressures, accelerations, angular rates and so forth. With a measurable amount of deformation having been obtained, electrical output signals can then be generated using the piezoresistive, piezoelectric or capacitive transduction effects. This latter field of research and technology has become known as MEMS (MEMS: micro-electro-mechanical systems) (2, 3).

Another important field of application that has benefited from MEMS methods and technologies is the field of thermal sensors (4). Thermal sensors are sensors that convert the input signals of interest into an intermediate thermal signal - usually a temperature change - that is electrically detected by performing a temperature measurement. The functional principle of such sensors is illustrated in Fig. 1. An indirect, two-step energy conversion process at first sight may seem unnecessarily complicated. However, it needs to be noted that it provides an easy workaround in all those cases in which semiconductors do not provide a useful solid-state effect for the special kind of signal transduction required. Such a situation, for instance, arises when thermal infrared radiation needs to be detected, i.e. photon energies that are significantly lower than the fundamental energy gap of most semiconductors. Thermopile sensors, for instance, are being used in such situations. At this point, however, it is also relevant to note that thermal sensors are not exotic workarounds around a few specific sensor problems, but rather constitute a very generic class of sensors in their own right. This generality derives from the fact that virtually any form of input energy can be dissipated into heat and therefore be electrically detected.

With regard to thermal sensors and actuators, gas sensors (5, 6) are a particularly interesting field of application as such sensors use resistance heating both for the purposes of actuation and sensing. This latter point reveals from the fact that chemical reactions at a sensor surface normally require thermal activation to proceed at a measurable rate. Once triggered, such surface reactions are able to generate or absorb quantities of heat that can be detected and therefore be used as a sensor signal. This possibility is used in catalytic gas sensors which are often called pellistors. Alternatively thermally activated surface

J. Webster (ed.), *Wiley Encyclopedia of Electrical and Electronics Engineering*. Copyright © 2007 John Wiley & Sons, Inc.

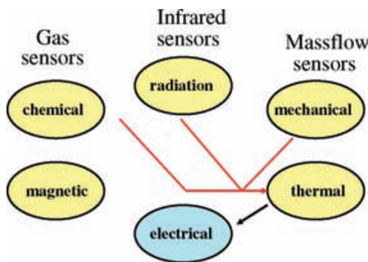

Fig. 1a Functional principle of thermal sensors. The nonelectrical input quantity to be sensed is converted into an intermediate thermal signal. This intermediate signal in turn is converted into the desired electrical output signal using a temperature measurement. Some application examples are noted in the top row.

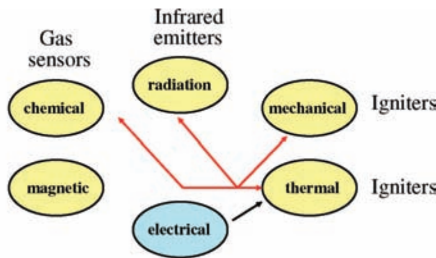

Fig. 1b Functional principle of thermal actuators. The nonelectrical output energy form is generated by dissipating electrical energy. The thermal energy in turn is converted into the output energy form. Application examples are noted in the figure.

reactions may produce conductance changes in special gas sensing layers. This latter sensing effect is used in metal oxide gas sensors.

THERMAL MICROSTRUCTURES

In order to operate thermal sensors and actuators efficiently, it is necessary to produce maximum temperature changes from a minimum amount of input energy. Temperature changes can be maximized by minimizing the mass to be heated. In this way its thermal capacitance is minimized. The other item to be considered is the thermal insulation of this mass. Insufficient insulation causes the generated heat to flow away and thus counteracts the requirement of minimizing the input power. As a key requirement we therefore recognize the importance of miniaturized structures that combine small heat capacitance with a high degree of thermal insulation. Such requirements can be fulfilled using thermal microstructures.

A specific example of a thermal microstructure is shown in Fig. 2. This microstructure consists of a thin dielectric membrane which is freely suspended within a massive silicon chip frame (7–11). Standard materials for forming such membranes are silicon oxide (SiO_2) and silicon nitride (Si_3N_4). Usually both materials are used in combination to arrive at a small level of tensile mechanical stress inside the suspended membrane. On top of this membrane a platinum (Pt) meander is formed for the heating of the membrane center. In order to avoid catalytic interactions with the heated Pt meander, the meander is covered by a thin, chemically inert layer of SiO_2. With Pt exhibiting

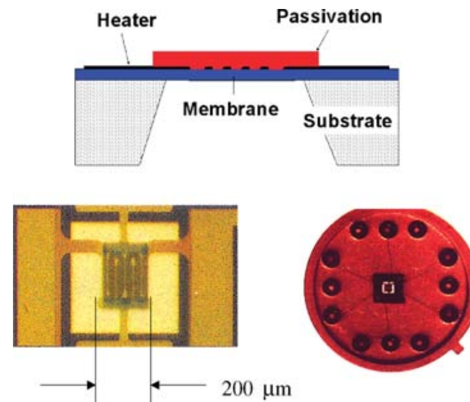

Fig. 2 Dielectric membrane-type heater elements. Top row: device cross-section, bottom row: top view onto membrane device; micro-heater chip as integrated into a TO-8 package.

a positive temperature coefficient of resistivity (TCR), the Pt meander can serve the double purpose of a heater and a temperature sensing element.

For thermal sensors, the usefulness of heated membrane devices builds on the following facts:

- The membrane center is thermally extremely well insulated from the surrounding chip frame. The high degree of thermal insulation results from the low thermal conductivity of the membrane materials and from the extreme aspect ratio of such dielectric membranes (lateral extension $\sim 500\ \mu$m; thickness $\sim 0.2\ \mu$m). Large temperature elevations can therefore be achieved with a minimum amount of input energy. This property is used in the following types of thermal sensors: bolometers (IR detection), thermopiles (IR detection), heat conductivity sensors (vacuum pressure sensors, gas sensors), catalytic gas sensors (detection of combustible gases), micro heaters for metal oxide gas sensors (detection of air contaminants, electronic noses);
- The inefficient heat transport through the dielectric membrane makes the device cooling very dependent on the properties of the surrounding gaseous ambient. This property is used in the following kinds of sensors: vacuum sensors, heat conductivity sensors (detection of H_2, CH_4 . . .), mass flow sensors (gas mixing, motor manage ment);
- Because of their very small volumes, the heat capacity of such membranes is extremely small. Heating and cooling rates on the order of 10^5 grad/s can be achieved. This latter property is of particular interest for the following kinds of sensors: fast mass flow sensors (motor management in automobiles, microdosing of gases and fluids. . .).

The membrane-type devices of Fig. 2 do not represent the only choice in designing thermal microstructures. Instead of using SiO_2 und Si_3N_4 as membrane materials, the silicon itself can be used to produce membrane-type devices out of massive silicon chips. Due to the roughly 100 times higher thermal conductivity of silicon relative

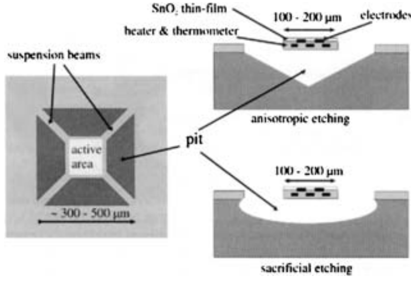

Fig. 3 Micro-heaters exhibiting a spider-like geometry. The heated membrane and its suspensions can be made out of bulk silicon either using anisotropic etching or porous silicon sacrificial layer technologies.

to SiO_2 and Si_3N_4, any heat conduction paths bridging the heated membrane centre with the cold silicon rim need to be geometrically constrained. Such geometrical constraints naturally lead to the spider-like geometries shown in Fig. 3 (11–18).

The disadvantage of high thermal conductivity of silicon membranes is offset by a number of advantages. With regard to sensors, one significant advantage is that electronic devices such as bipolar and field-effect transistors can be integrated into the thermally insulated membranes. This possibility significantly enhances the capabilities of producing higher-functionality sensor devices (13, 16–18). Considering thermal actuators, the following advantages are relevant: firstly, bulk silicon microstructures exhibit considerable mechanical stability; secondly, heavily doped bulk silicon can be used as an active heater material with excellent high-temperature stability (operation temperatures up to 800°C) and thirdly, when heated beyond its intrinsic temperature, heavily doped bulk silicon can exhibit the phenomenon of "explosive evaporation". Whereas the first two properties are relevant for gas sensors and thermal IR emitters, the latter property is particularly useful for realizing one-shot thermal actuators such as airbag igniters.

In the examples below we show how these individual characteristics of micro heaters can be used to arrive at a range of industrially important sensor and actuator devices.

SPECIFIC SENSOR APPLICATIONS

Heat Conductivity Sensors

Heat conductivity sensors use the fact that the electrical power consumption of a dielectric membrane sensitively depends on the heat conductivity of the ambient air. The physical properties that become amenable to measurement in this way can be read off from the formula for the heat conductivity of an ideal gas. In general terms the heat conductivity is given by (19):

$$\lambda_{air} = \frac{1}{3} \cdot C_V \cdot v_{av} \cdot \Lambda_{av} \tag{1}$$

C_V : specific heat at constant volume
v_{av} : average molecular velocity .
Λ_{av} : average mean free path

In general the average mean free path Λ_{free} is solely determined by the gas-kinetic parameters pressure P, temperature T and the collision cross section σ_s:

$$\Lambda_{free} = \frac{k_B \cdot T}{\sigma_s \cdot P} \tag{2}$$

k_B : Boltzmann's constant
T : absolute temperature
P : ambient temperature
σ_s : molecular cross section.

In those situations in which the molecular motion is geometrically constrained to a characteristic length L_c, as for instance by the distance of the heated membrane from the device package, the average mean free path Λ_{av} may be reduced below Λ_{free}:

$$\frac{1}{\Lambda_{av}} = \frac{1}{\Lambda_{free}} + \frac{1}{L_c}. \tag{3}$$

Introducing a pressure parameter characterizing geometrically constrained situations,

$$P_c = \frac{k_B \cdot T}{\sigma_S \cdot L_c}, \tag{4}$$

the thermal conductivity λ_{air} of the ambient air can be expressed as:

$$\lambda_{air}(P, P_c, M_{rel}, T) = \frac{5}{3} \cdot \left(\frac{2 \cdot k_B^3 \cdot T}{\pi \cdot M_{rel} \cdot M_0 \cdot \sigma_s^2} \right)^{\frac{1}{2}} \cdot \left(\frac{P}{P + P_c} \right) \tag{5}$$

M_0 : atomic mass unit(AMU)
M_{rel} : relative molecular mass

From this latter equation it is evident that in the absence of geometrical constraints ($L_c \to \infty$), the heat conductivity does not depend on the pressure P. In the case of constraints, the heat conductivity decreases as the pressure is decreased.

Fig. 4 presents results for the geometrically constrained heat conductivity of air as a function of the ambient air pressure. In this example it has been assumed that the motion of the air molecules is confined to the depth of a typical etch trough inside a thermal microstructure, i.e. $L_c = L_{wall} \sim 300\ \mu m$. As revealed from Fig. 4 this constraint becomes relevant when the air pressure is reduced to about 100 Pa, i.e. to about one thousandth of the normal air pressure. Above this pressure the heat conductivity is independent of P but dependent on the average molecular mass (Fig. 4a) and on the gas temperature (Fig. 4b). Below about 10 Pa the heat conductivity additionally becomes linearly dependent on P.

The above results can be used in two ways: in the range of normal ambient pressures the dependence of the average molecular mass can be used to detect gases in air whose molecular mass differs from the average molecular mass of air (20). In the low pressure range heated membrane devices can be used to measure the pressure inside vacuum vessels. A principle device architecture that is useful in both cases is shown in Fig. 5.

Turning to the gas sensing application first we note that clean air consists of about 80% N_2 (M_{rel} = 28) and 20% O_2

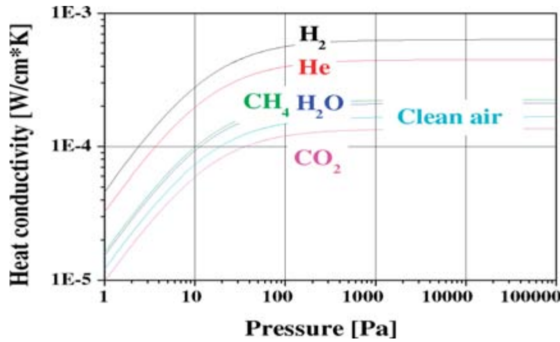

Fig. 4a Geometrically constrained heat conductivity of clean air as a function of pressure. Data for H_2, He, CH_4, H_2O and CO_2 are shown for comparison.

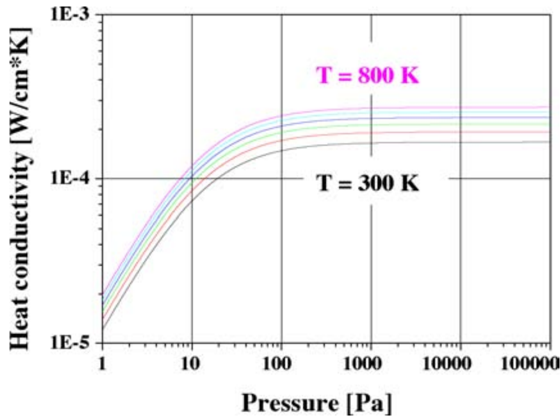

Fig. 4b Geometrically constrained heat conductivity of clean air (M_{rel} = 28.8) as a function of pressure. Parameter: ambient air temperature.

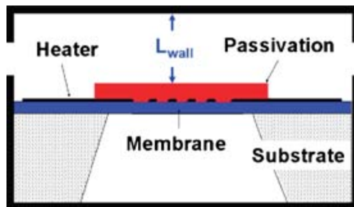

Fig. 5 Principle architecture of a heat conductivity sensor. At normal ambient pressure it can be used to detect the presence of combustible gases (H_2, CH_4) in air. At low pressures, in which the mean free path is constrained by L_{wall}, it can be used to measure the vacuum pressure.

(M_{rel} = 32); the average molecular mass of clean air therefore turns out to be $M_{rel} \sim 28.8$. Reference to the data of Fig. 4a shows that those gases with molecular masses lighter than this should easily be detectable. In this class of gases we find combustible gases such as H_2 and CH_4, i.e. combustible gases that represent safety hazards when their concentration exceeds their lower explosive limits (LEL) of about 4% in air.

For detection, a heated membrane device is used as in Fig. 5 but with the gas inlet and outlet ports being closed by porous membranes. This porous sealing allows for a diffusive gas exchange but it does not allow an ignition process to initiate should the LEL concentration be exceeded. For detection the membrane device is heated above the ambient temperature and kept constant by an electronic control circuit.

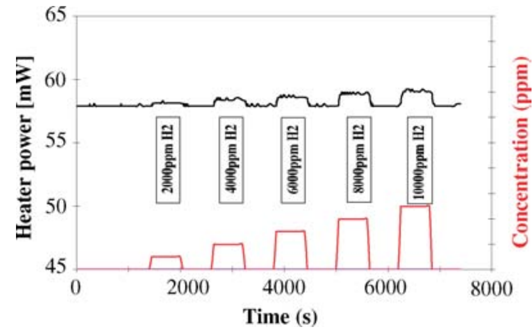

Fig. 6 Output signal of a heated membrane-type sensor in response to increasing concentrations of H_2 (red). Because of the lower average molecular mass, additional heat needs to be supplied to the heated membrane during each H_2 exposure pulse.

With this kind of control being established and gases of low molecular weight entering the sensor package, more electrical power needs to be fed into the membrane heater to maintain a constant surface temperature. This excess power consequently can be used as a sensor output signal. The data in Fig. 6 show that in this way H_2 can be detected in concentrations far below the LEL of H_2 of 4% or 40,000ppm respectively. A likely application scenario in the near future will be H_2 driven cars, where safety requires all components of the power train to be monitored for H_2 leakages.

The data of Fig. 7 point out a problem that is commonly encountered in the field of chemical sensors, i.e. cross sensitivity. It shows that heat-conductivity sensors not only detect H_2 but also a range of other gases provided two conditions are met: (i) the gas concentration needs to exceed the minimum detectable concentration of about 1000 ppm and the gases need to have a molecular mass that is different from the average mass of clean air, i.e. $M_{rel} \sim 28.8$. Such conditions are particularly true in the case of H_2O vapor. As the heat conductivity is further dependent on temperature (see Fig. 4b), it is evident that heat conductivity sensors require both temperature and humidity compensation in order to be useful. Discrimination of several gases becomes possible employing sensor array concepts (26).

Turning to the second application, namely vacuum pressure sensors, Fig. 4 shows that this is possible at pressures at which the mean free path becomes constrained by the dimensions of the micro-heater device. In the example considered in Fig. 4 we assumed that the distance between the heated membrane and the package is on the order of a typical silicon wafer thickness ($L_{wall} \sim 300\mu$m). Such macroscopic air gaps can also be realized without invoking MEMS technologies. Macroscopic versions of heat conductivity sensors are currently in wide-spread use in the field of vacuum technology and they are well known under the name of Pirani gauges. Making use of MEMS technologies and realizing very small gaps in the order of 1 μm or less between the heated membrane and a neighboring cold wall, the condition of geometrically constrained mean free paths can already be met in the range of normal ambient pressures. MEMS thermal conductivity sensors therefore can

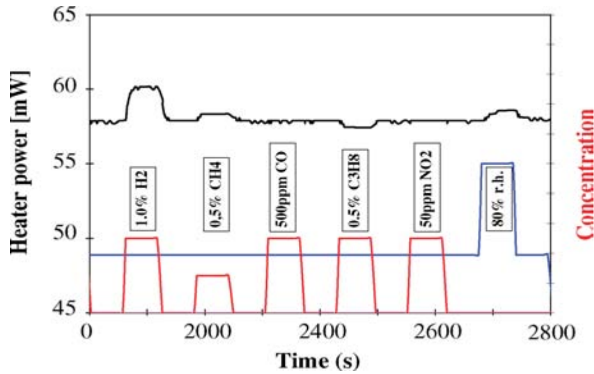

Fig. 7 Response of a heat conductivity sensor towards a range of gases which might interfere with H_2 detection. Such cross sensitivities arise from the fact that heat conductivity detects the physical property “average molecular mass" rather than molecular identity.

also be used for measurements in the meteorologically relevant range of air pressures. For such sensors all the above considerations concerning cross sensitivity are relevant. As in a meteorological measurement the ambient temperature and the humidity are being measured alongside with the air pressure, temperature and humidity compensation are of no concern in this particular application.

Mass Flow Sensors

Another important field of application of heated-membrane devices are mass flow sensors in automobiles (21–27).

There mass flow sensors help regulating the flow of air into internal combustion engines. Such a control is needed to inject stoichiometric mixtures of air and fuel into the cylinders. This in turn allows for an optimum after-treatment of the exhaust gases in the commonly applied three-way catalysts. Whereas the fuel injection is performed directly into the cylinders, the stoichiometrically equivalent amount of air is taken into the engine via a so-called throttle valve. The position of this valve globally regulates the air-intake into all the cylinders (Fig. 8) and thus controls the average demand of air to be injected into the cylinders. In order for such a control to be exerted, the amount of air passing the throttle valve is measured by a hot-wire anemometer. Such an anemometer in principle consists of a piece of heated Pt wire that is cooled by the flowing air. This cooling effect in turn is a measure of the air flow that can be detected via a change in the Pt heater resistance.

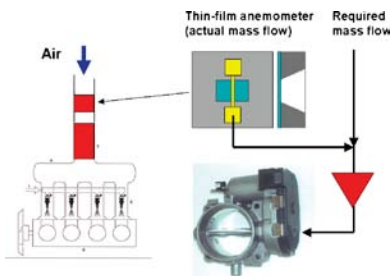

Fig. 8 Control of air mass flow into an internal combustion engine using a micro-machined hot-film anemometer.

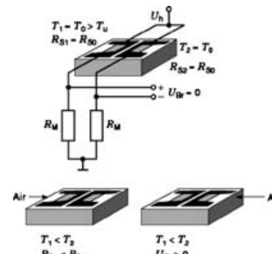

Fig. 9a Electronic circuit to detect air mass flow using a two-wire anemometer.

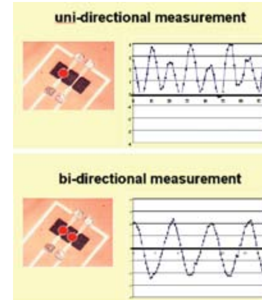

Fig. 9b Uni-directional and bi-directional response to a vibrating air column upon heating one (top panel) or two wires (bottom panel).

The interest in micromechanical versions of hot-film anemometers stems from the fact that these can exhibit very short thermal response times. Thermal response times can be as small as 5 msec when operated in the vicinity of 400°C. Such a high speed of air flow monitoring is required by the fact that - in certain revolution ranges - the pumping action of the internal combustion engine can lead to oscillations in the air inlet system. In such a situation the vibrating air column performs periodic forward/backward movements above the sensor surface. In such an event the injected air flow can be seriously overestimated once an unidirectional flow measurement is made. An exact monitoring, however, can be realized by performing a bi-directional monitoring of the air flow. To this end, a heated membrane device with two parallel Pt wires running across a dielectric membrane is required. A sensor device with a two-wire architecture is shown in Fig. 9. This figure also presents sensor output data that were generated in response to a vibrating air column generated by a loudspeaker. Fig. 9b shows that the amount of air flow can be monitored using a single hot wire; heating both wires, the direction of the air flow can additionally be determined. It is under these latter conditions that a correct injection of the air into an internal combustion engine can be realized.

A detailed mathematical analysis of the sensor behavior can be obtained using the convection equation. This equation is a generalization of the normal heat conduction equation to the situation of a moving air flow. The analysis is lengthy but straight-forward and ultimately leads to the well-known King's law of anemometers (22):

$$P_{el}(v, T, P) = \alpha(T, P) \cdot \sqrt{v} + \beta(T, P) \quad (6)$$

This law states that the electrical power P_{el} that needs to be fed into a constant-temperature operated heated-wire anemometer should scale with the square root of the air velocity. As the constants α and β in equation 6 depend both on the temperature T and the pressure P of the ambient air, both T and P need to be measured independently along with the air velocity to obtain the desired information about the air mass flow. In the car industry such flow monitoring systems have found wide-spread application and are being produced nowadays in quantities of several millions/per year (26, 27).

SPECIFIC ACTUATOR APPLICATIONS

Micro heaters for metal oxide gas sensors

Metal oxide gas sensors are widely used in air quality and safety monitoring applications. Metal oxides are a class of semiconductor materials that respond to the presence of adsorbed molecules via conductivity changes (5, 6). Most of these materials are n-type, i.e. gas-induced conductivity changes are due to changes in the sub-surface electron density. Adsorbed molecular species can induce both increases as well as decreases in the surface conductance. A few molecules, which are more strongly oxidizing than molecular oxygen ($O_3, NO_2, SO_2, \ldots$), tend to withdraw electrons from the sub-surface region. Most other molecules, however, reduce the sensor surface and thus cause the surface conductivity to increase. In such detection events the adsorbed analyte molecules undergo surface combustion events in which pre-adsorbed negative oxygen ions are consumed and in which the trapped electrons are returned to the metal oxide conduction band. A common property of all these detection reactions is that they require significant levels of thermal activation to proceed at a measurable rate. It is at this point that micro-heating comes in. In the case of metal oxide gas sensors micro-heaters perform an actuator function in that they enable the very detection reactions to proceed at the surface of a gas-sensitive semiconductor layer.

To date most commercial metal oxide gas sensors are prepared by means of screen printing onto bulk ceramic substrates (28, 29). Due to their bulky nature, ceramic heater substrates consume heating powers on the order of 0.5 - 1W per sensor element for attaining the required operation temperatures of about 400°C. This high level of power consumption represents a severe draw-back when metal oxide gas sensors are to be used in bus-connected sensor networks or when sensor arrays with higher levels of gas distinction are to be realized.

Sensor arrays like the one shown in Figs. 10a–d cannot detect the molecular identity of gases as such. The two sensor output signals simply characterize the oxidizing or reducing power of the reactive gases that abound in the ambient atmosphere. In this sense the two-dimensional sensor output signals simply represent “smell patterns” that are characteristic of the individual gases and gas mixtures. This capability of distinguishing smell patterns can, for in-

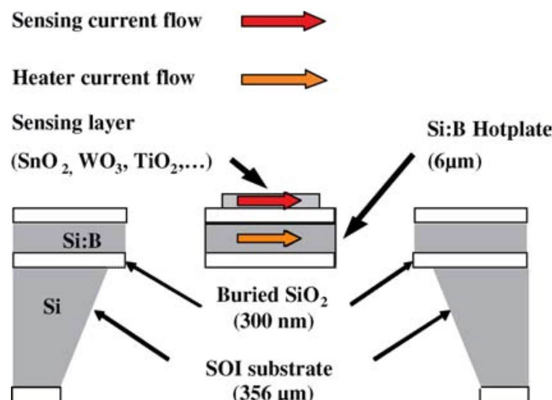

Fig. 10a Device cross section of SOI micro-heaters. The heater current is passed through a heavily doped silicon bridge, which carries the gas-sensitive sensor layers.

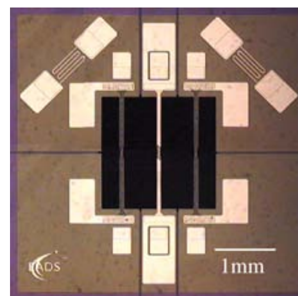

Fig. 10b SOI-based gas sensor array featuring two metal oxide gas sensors and a thermally insulated Pt thermometer.

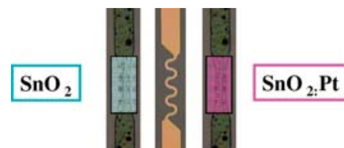

Fig. 10c Close-up view onto the heater bridges of the sensor array chip in Fig. 10b. The outer bridges carry different kinds of gas sensing layers and the center one a fast Pt thermometer.

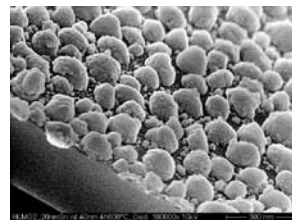

Fig. 10d Nano-granular SnO2 as deposited onto one of the heater bridges of the sensor array in Fig. 10b.

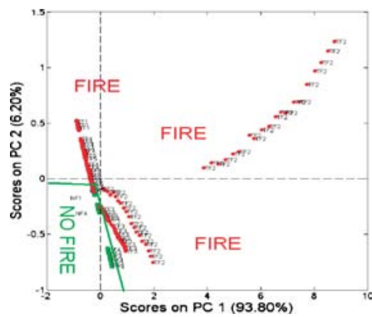

Fig. 11 Response of the above two-sensor array towards different fire and non-fire situations. TF and NF stand for well-defined fire and non-fire situations as generated in a standardized test procedure.

stance, be used to detect fires (39). The data presented in Fig. 11 show that in this way different "fire" and "non-fire" scenarios can be distinguished. In the future such metal oxide gas sensor arrays are likely to be combined with the currently used types of smoke detectors to arrive at lower levels of false-alarm rates.

Thermal infrared emitters

A high-selectivity method of gas detection is non-dispersive infrared (NDIR) absorption. This method detects characteristic molecular vibrations of polar molecules and thus represents a spectroscopic method of gas detection. NDIR systems require as key components bright thermal IR sources that can be modulated at reasonably high speed to allow high-sensitivity lock-in detection to be applied. In addition such sources should also provide a stable IR emission - unaffected both by short-term environmental changes as well as by long-term drift (40, 41). As miniaturized light bulbs, widely used in commercial NDIR gas sensing systems, cannot fulfill such requirements, thermal micro-heaters have been developed that can live up to such requirements. Examples of such emitters are shown in Fig. 12 (42).

The emitters in Fig. 12 use the same kind of SOI base technology as in the metal oxide gas sensors above. Due to the different actuator requirements, however, these latter devices exhibit a much different geometry. Whereas tiny hot spots are sufficient to heat metal oxide gas sensing layers to their appropriate operation temperature, the heated area in IR emitting devices needs to be made much larger to generate a sufficiently large radiation output. The heated area, on the other hand, cannot be increased beyond limits as larger heated areas increase the thermal response time of the emitters and thus reduce their maximum modulation speed. Requirements for a sufficiently high modulation speed arise from the request of obviating bulky and expensive mechanical choppers in the NDIR systems. Both conflicting requirements lead to relatively large hotplates with heated areas of $1.5 \times 1.5\ mm^2$.

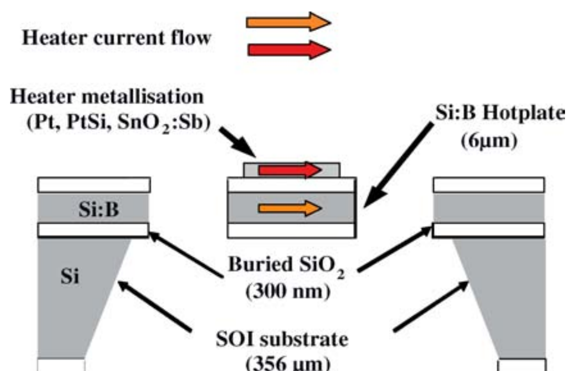

Fig. 12a Device cross section of SOI-based thermal IR emitters. The heater current can either be passed through the heavily doped silicon hotplate or through specific heater metallizations deposited on top of the hotplate.

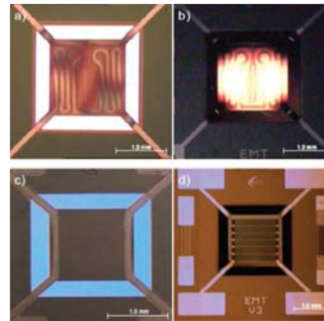

Fig. 12b Different versions of SOI-based thermal emitter devices: (a) Pt heater meander, (b) Pt emitter operated at around 800°C, (c) device with an area heater of bulk silicon (Si:B) (d) device with an area heater consisting of deposited SnO2:Sb.

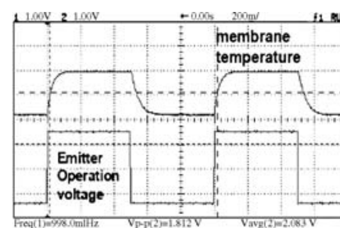

Fig. 13a Response of the surface temperature of the hotplate IR emitters to rectangular drive voltage pulses with 1Hz repetition frequency. Maximum modulation frequencies are on the order of 10 Hz.

Fig. 13 presents some device characteristics of the emitters shown in Fig. 12. Fig. 13a shows how the surface temperature of the hotplates responds to rectangular changes in the heater driver voltage. These data reveal that thermal response times are on the order of 100ms, i.e. possible modulation speeds go up to 10 Hz, which is enough for operating conventional and photoacoustic NDIR systems in an efficient manner (43).

Fig. 13b, on the other hand shows that the emitted radiation peaks at around 4-5 μm, thus allowing for efficient NDIR detection in the 3-5 μm atmospheric window. A final, but important point to note is that SOI-based IR emitters exhibit a vastly improved long-term stability with regard to earlier dielectric membrane-type devices: accelerated degradation tests have indicated that SOI emitters can exhibit lifetimes up to 10 years when operated at temperatures approaching 1000°C (44).

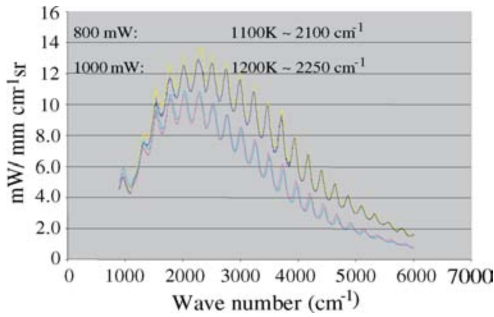

Fig. 13b IR power as a function of the wave number for the emitted radiation. The interference fringes arise from reflections at the upper and lower silicon / air boundaries of the Si:B emitter membranes.

Airbag igniters

An actuator application of micro-heaters that promises a large market potential are airbag igniters. Airbags are an important safety feature in modern cars (45, 46). Whereas a single airbag was installed in early cars, up to two dozens of airbags are installed nowadays. Depending on the intensity and direction of the impact, the individual airbags need to be triggered in a way that promises to minimize the effect of the impact. Building such complex safety systems requires electronic airbag igniters that exhibit highly reproducible properties and that lend themselves towards integration into safety bus systems. Semiconductor technologies are best suited towards solving this problem: firstly because silicon technology offers the required precision and secondly because batch processing promises low cost. With regard to the thermal IR emitter presented above, airbag igniters are one-shot devices that become irreversibly destroyed when used. During use such igniter devices have to generate within a very short time temperatures much larger than the thermal IR emitters and they also need to generate an intense mechanical shock wave during the ignition event. These latter requirements can also be satisfied using silicon microstructures as these can exhibit the phenomenon of "explosive evaporation".

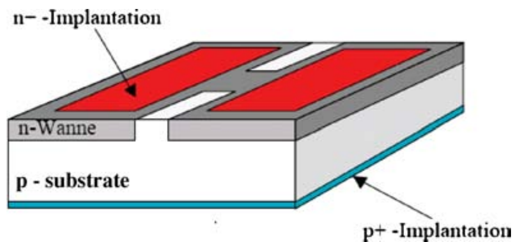

Fig. 14a Schematic layout of the silicon bridge igniter.

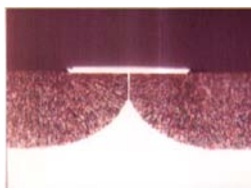

Fig. 14b N-type silicon bridge thermally insulated from the p-type substrate by porous silicon formation.

Whereas in principle the phenomenon of explosive evaporation can also be observed in SOI-based devices, igniter devices have to comply with the additional technical constraint of very low cost. Such boundary conditions can be met using porous silicon technology for forming the thermally insulated structures inside silicon chips. The semiconductor device used in this latter case is shown in Fig. 14. Fig. 14a schematically indicates that the igniter device basically consists of a heavily doped n-type silicon bridge formed at the surface of a moderately doped p-type silicon wafer. Such bridges can be formed by ion implantation and a subsequent drive-in diffusion. In a second step the doped silicon bridge is thermally insulated by forming porous silicon in all those surface areas that were not converted to n-type conductivity. Fig. 14b shows that in this way the doped silicon bridge becomes successively under-etched and thermally insulated by porous silicon as the etching proceeds from the unmasked surface areas.

The thermal insulation provided by the porous silicon layer causes Joule heat to pile up inside the silicon bridge when current is passed through it. Fig. 15a shows that the porous silicon layer provides enough thermal insulation to allow heating the silicon bridge well beyond its melting point ($T_m \sim 1412^{\circ}C$). Melting and re-condensation of evaporated silicon is evidenced by the small silicon spheres deposited on the damaged substrate.

The phenomenon of explosive evaporation is further demonstrated by the data of Figs. 15b–d. Figs. 15b and c show the current and light transients that occur during bridge heating. Fig. 15c, in particular, shows in greater detail that a sharp current increase is observed after a short constant-current period (~200μs). This time delay corresponds to the time required for heating the bridge to its intrinsic temperature. After this temperature has been

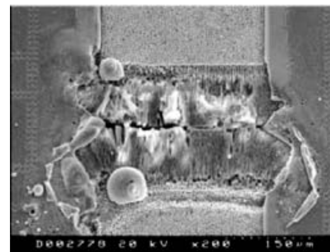

Fig. 15a View onto an ignited bride showing re-condensed silicon particles.

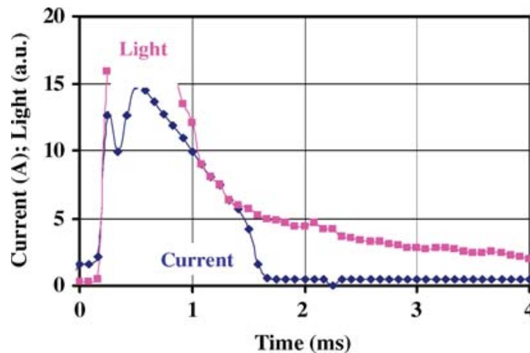

Fig. 15b Current and light transients during ignition of the silicon bridge.

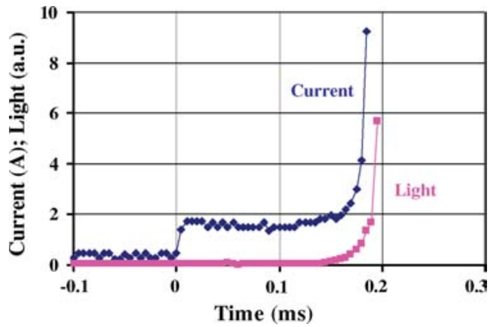

Fig. 15c Detail view onto the current and light transients of Fig. 15b showing more clearly the ignition delay.

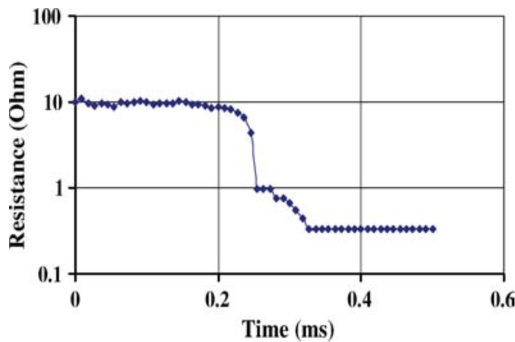

Fig. 15d Variation of the bridge resistance during the ignition process.

reached, the exponentially increasing conductivity of the silicon bridge causes large amounts of current ($>> 1A$) to be passed through the tiny silicon bridge and huge amounts of heat to be generated there. As due to the thermal insulation this heat cannot be conducted away from the bridge, a rapid thermal runaway occurs, leading to the phenomenon of explosive evaporation. This latter interpretation is corroborated by Fig. 15d which displays the resistance variation as derived from the current and voltage transients that can be observed during the ignition process. From the electrical and geometrical data of the device it can further be figured out that peak power densities on the order of $P_{max} \sim 10^8 W/cm^3$ are generated. In this way peak temperatures up to 3000°C may be attained and a mechanical shock wave is initiated as the evaporated silicon suddenly requires roughly 1000 times more space than the initial silicon bridge. Such conditions are favorable for triggering explosive charges as in airbag safety devices.

MATHEMATICAL MODELING OF THERMAL MICROSTRUCTURES

Designing and optimizing thermal microstructures requires state of the art finite element modeling tools. The principle behavior of sensor and actuator devices, however, can be rationalized in an efficient way by using thermal equivalent circuits (4–40). The idea of thermal equivalent circuits can be derived in a straight-forward way from the heat conduction equation. Such considerations lead to the result that there are direct analogies between electrical and thermal properties:

Electrical domain		**Thermal domain**
Voltage (V)	↔	Temperature (K)
Current (A)	↔	Heat flow (W)
Resistance (Ω = V/A)	↔	Thermal resistance (K/W)
Capacitance (F)	↔	Thermal capacitance (Ws/K)

Following this idea a heated membrane device like the one shown in Fig. 2 can be modeled as indicated in Fig. 16.

In this picture we assume that the membrane center is homogenously heated to a temperature $T_m > T_a$ and that no heat is generated in the periphery of the membrane that bridges the heated membrane center with the cold silicon rim, maintained at the ambient temperature T_a. Heat conduction from this membrane center can then occur via three independent processes: (i) solid-state heat conduction through the membrane, (ii) heat conduction (convection) through the ambient air and (iii) heat radiation. Each of these processes can be associated with equivalent thermal resistors whose magnitude depends on the temperature difference ($T_m - T_a$), as well as on the thermal and geometrical properties of the heat transporting medium that bridges the gap between the heated membrane center and its cold surroundings. In this picture the resulting overall thermal resistance arises from the parallel combination of

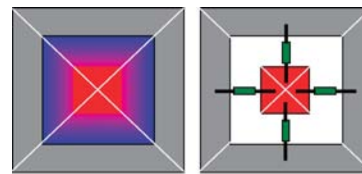

Real temperature distribution on top of a dielectric membrane with a homogeneously heated center

Modeling of solid-state heat flow through the outer parts of the membrane using thermal resistors

Fig. 16a Thermal resistor modeling of the heat flow from a homogeneously heated membrane towards the cold silicon rim.

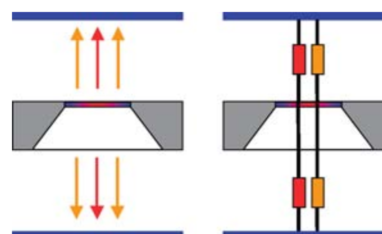

Thermal losses due to molecular heat conduction in the ambient air and thermal radiation.

Modeling of heat conduction in air and thermal radiation using thermal resistors.

Fig. 16b Thermal resistor modeling of the heat flow from a homogeneously heated membrane towards its neighboring heat sinks.

the individual thermal resistances:

$$\left(\frac{1}{R_{th}\left(T_m - T_a\right)}\right) = \left(\frac{1}{R_{solid}\left(T_m - T_a\right)}\right) + \\ + \left(\frac{1}{R_{air}\left(T_m - T_a\right)}\right) + \left(\frac{1}{R_{rad}\left(T_m - T_a\right)}\right) \quad (7)$$

With this result the temperature difference $T_m - T_a$ derives as:

$$T_m - T_a = R_{th}(T_m - T_a) \cdot P\,in \quad (8)$$

This latter result shows that a high thermal resistance minimizes the input power P_{in} for attaining a certain membrane temperature T_m. Furthermore this result shows that the actual value of T_m depends on T_a, i.e. on the ambient temperature in which the micro-heater is being operated in. In the analogy introduced above, the temperature baseline value of T_a corresponds to the zero-potential baseline in the equivalent electrical circuit.

Quantitatively the individual resistances can be expressed as follows:

- ***Thermal resistance due to solid-state heat conduction inside the membrane:***

$$R_{solid} = \left(\frac{1}{4}\right) \cdot \left(\frac{1}{\lambda_{solid}}\right) \cdot \left(\frac{L_{bridge}}{t_m \cdot W_{bridge}}\right) \quad (9)$$

λ_{solid}: thermal conductivity of membrane material
L_{bridge}: length of non – heated bridging rim of membrane
W_{bridge}: effective width of non – heated bridging rim of membrane
t_m : thickness of membrane

The factor of $\frac{1}{4}$ derives from the fact that heat is dissipated into four bridging resistors at all four sides of the heated membrane center.

- ***Thermal resistance due to heat conduction in air:***
The heat conductivity of an ideal gas is given by:

$$\lambda_{air} = \frac{5}{3} \cdot \left(\frac{2 \cdot k\,B^3 \cdot T}{\pi \cdot M_{rel} \cdot M_0 \cdot \sigma_s^2}\right)^{\frac{1}{2}} \quad (10)$$

k_B : Boltzmann's constant
M_0 : atomic mass unit (AMU)
M_{rel} : relative molecular mass
T : absolute temperature
σ_s : cellison cross section of molecules.

The total thermal resistance due to heat conduction derives from the parallel combination of the thermal resistances representing the heat conduction processes at the top and bottom surfaces of the heated membrane:

$$R_{th_air_top} = \left(\frac{1}{\lambda_{air}}\right) \cdot \frac{L_{top}}{L_m^2} \quad (11a)$$

$$R_{th_air_bottom} = \left(\frac{1}{\lambda_{air}}\right) \cdot \frac{L_{bottom}}{L_m^2} \quad (11b)$$

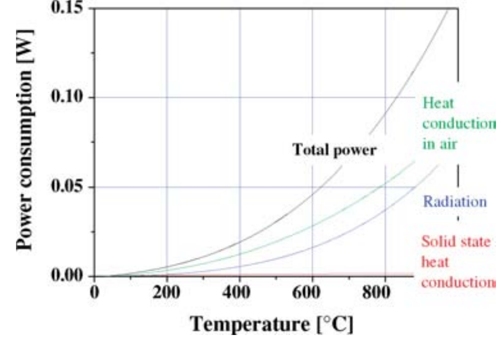

Fig. 17a Calculated heating power consumption for a membrane-type heater as shown in Fig. 2. The individual contributions due to dissipation into solid-state heat conduction, heat transport in air and thermal radiation are indicated.

L_{top}, L_{bottom} : distance between the heated membrane and heat sinks at the top and bottom sides opposite to the heated membrane area

L_m : lateral extent of heated membrane area

- ***Thermal resistance caused by emission of thermal black-body radiation:***
With the center of the membrane being heated to a temperature T_m and the surrounding heat sinks being maintained at a temperature T_a, the net energy flow between the heated membrane and the surrounding heat sinks is

$$J_{rad}(T_m - T_a) = \sigma_{SB} \cdot (T_m^4 - T_a^4) \\ \sigma_{SB} : \text{Stephan–Boltzmann radiation constant} \quad (12)$$

With this result, the thermal resistance caused by the emission of black-body radiation becomes

$$R_{th_rad}(T_m - T_a) = \frac{1}{2} \cdot \left[\frac{T_m - T_a}{L_m^2 \cdot \sigma_{SB} \cdot \left(T_m^4 - T_a^4\right)}\right] \quad (13)$$

The factor ½ derives from the fact that the same amount of radiation is emitted from both the top and bottom surfaces toward the respective heat sinks.

In thermal equilibrium these individual cooling processes need to be compensated for by the electrical power input into the membrane center. Fig. 17a shows how these individual cooling processes contribute to the total power consumption of the device. Fig. 17b shows how the thermal response time τ_{th} of the device varies as T_m is increased. This decrease in τ_{th} is due to the rapidly increasing cooling effects due to heat conduction and heat radiation.

So far our considerations have been confined to the thermal insulation provided by a thermal microstructure. A high thermal resistance minimizes the input power for attaining a certain temperature difference $(T_m - T_a)$ and thus optimizes the sensitivity of a thermal sensor device. Another sensor property that is important is the thermal response time, which limits its capability to follow time-varying signals. In analogy to the equivalent electrical circuit, this response time is given by:

$$\tau_{th} = R_{th} \cdot C_{th} \quad (14)$$

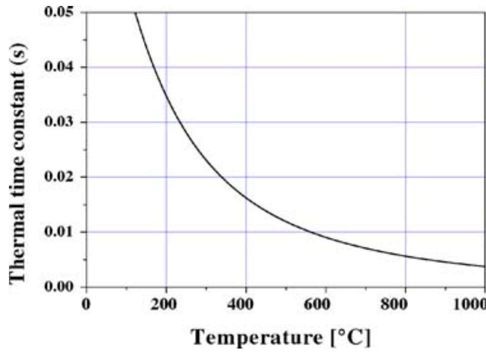

Fig. 17b Thermal time constant as a function of the membrane temperature. The time constant drops with increasing membrane temperature due to the increasing thermal losses due to heat conduction in air and due to thermal radiation.

In this equation, C_{th} stands for the thermal capacitance. This capacitance in turn depends on the solid-state properties and on the geometry of the membrane material:

$$C_{th} = \rho_{solid} \cdot C_{p_solid} \cdot L_m^2 \cdot t_m \quad (15)$$

ρ_{solid} : mass density of membrane material
C_{p_solid} : heat capacity at constant pressure of membrane material

In case R_{th} is limited by R_{solid}, τ_{th} becomes

$$\tau_{th} = \left(\frac{\rho_{solid} \cdot C_{p_solid}}{\lambda_{solid}}\right) \cdot \left(\frac{L_{bridge}}{W_{bridge}}\right) \cdot \left(L_m^2\right) \quad (16)$$

Looking at this latter result, we note that τ_{th} depends on three items:

(i) The solid-state properties of the membrane material
(ii) The geometry of the suspensions that provide thermal insulation
(iii) The magnitude of the heated area.

Whereas small heated areas clearly minimize τ_{th} (iii), optimizing items (i) and (ii) to the end of obtaining small values of τ_{th} is clearly in conflict with good thermal insulation. This conflict is the thermal analog of the gain-bandwidth limitation in conventional electrical engineering.

BIBLIOGRAPHY

1. R. Waser:" *Nanoelectronics and Information Technology*"; Wiley-VCH, Weinheim 2003, ISBN 3527403639.
2. S. M. Sze: " *Semiconductor Sensors*"; John Wiley & Sons, New York, Chichester (1994), ISBN 0-471-54609-7.
3. A. Heuberger: " *Mikromechanik*"; Springer-Verlag, Berlin, Heidelberg, New York (1989) ; ISBN 3-540-18721-9.
4. G. C. M. Meyer, A. W. van Herwarden: " *Thermal Sensors*"; Institute of Physics Publishing; Bristol and Philadelphia; ISBN 0-7503-0220-8.
5. P. T. Moseley, B. C. Tofield: " *Solid State Gas Sensors*", Adam Hilger, Bristol, 1987.
6. P. T. Moseley, J. Norris, D. E. Williams: " *Techniques and Mechanisms in Gas Sensing*", Adam Hilger, Bristol, 1991.
7. J. S. Suehle, R. E. Cavicchi, M. Gaitan, S. Semancik: " Tin Oxide Gas Sensor Fabricated Using CMOS Micro-Hotplates and in-situ Processing"; *IEEE Electron Device Letters* **14** (1993) 118–120.
8. S. Semancik, R. E. Cavicchi, M. C. Wheeler, J. E. Tiffany, G. E. Poirier, R. M. Walton, J. S. Suehle, B. Panchapakesan, D. L. DeVoe, " Microhotplate Platforms for Chemical Sensor Research," *Sensors & Actuators* **B3923**, (2001), 1–13.
9. G. Sberveglieri, W. Hellmich, G. Müller: " Silicon Hotplates for Metal Oxide Gas Sensor Elements", *Microsyst. Technol* **3** (1997) 183–190.
10. D. Vincenzi, M. A. Butturi, V. Guidi, M. C. Carotta, G. Martinelli, V. Guarnieri, S. Brida, B. Margesin, F. Giacomozzi, M. Zen, D. Giusti, G. Soncini, A. A. Vasiliev, A. V. Pisliakov: " Gas-Sensing Device Implemented on a Micromachined Membrane: A Combination of Thick-Film and VLSI Technologies", *Proc. 8th International Meeting on Chemical Sensors*,Basel (Switzerland) 2000.
11. S. Fung, Z. Tang, P. Chan, J. Sin, P. Cheung: " Thermal Analysis and Design of a Micro-Hotplate for Integrated Gas Sensor Applications"; *Proc. Transducers '95, Eurosensors IX*, Stockholm, Sweden (1995), pp 818–821.
12. Cs. Düsco, E. Vaszsonyi, M. Adam, I. Barsony, J. G. E. Gardeniers, A. van den Berg: " Porous Silicon Bulk Micromachining for Thermally Isolated Membrane Formation"; *Proc. Eurosensors X, Leuven*, Belgium (1996), pp 227–230.
13. J. W. Gardner, J. A. Covington, F. Udrea, T. Dogaru, C. C. Lu, W. Milne, " SOI-Based Micro-Hotplate Microcalorimeter Gas Sensor with Integrated BiCMOS Transducer", *Proceedings Transducers '01 — Eurosensors XV*, 2001, pp 1688–1691.
14. A. Friedberger, P. Kreisl, E. Rose, G. Müller, G. Kühner, J. Wöllenstein, H. Böttner: " Micromechanical Fabrication of Robust Low-Power Metal-Oxide Gas Sensors". *Sensors & Actuators* **B93** (2003) 345–349.
15. G. Müller, A. Friedberger, P. Kreisl, O. Schulz, Th. Becker: " A MEMS Toolkit for Metal-Oxide-Based Gas Sensing Systems"; *Proc. III Int. Seminar on Semiconductor Gas Sensors*,Ustron, Poland, Sept. 2002; *Thin Solid Films* **436** (2003) 34–45.
16. D. Barrettino, M. Graf, W. H. Song, K.-U. Kirstein, A. Hierlemann, H. Baltes: " Hotplate-Based Monolithic CMOS Microsystems for Gas Detection and Material Characterization for Operating Temperatures up to 500°C.", *IEEE Journal of Solid-State Circuits*, **39**, No. 7, pp 1202–1207, 2004.
17. P. Kreisl, A. Helwig, A. Friedberger, G. Müller, E. Obermeier, S. Sotier: " Detection of Hydrocarbon Species Using Silicon MOS capacitors Operated in a Non-Stationary Temperature Pulse Mode". *Sensors & Actuators* **B106** (2005) 489–497.
18. P. Kreisl, A. Helwig, G. Müller, E. Obermeier, S. Sotier: " Detection of Hydrocarbon Species Using Silicon MOS Field Effect Transistors Operated in a Non-Stationary Temperature-Pulse Mode". *Sensors & Actuators* **B106** (2005) 442–449.
19. Ch. Kittel: " *Thermal Physics*"; J. Wiley & Sons, ISBN 978-0716710882.
20. P. Tardy, J.-R. Coulon, F. Menil: " New Type of Thermal Conductivity Sensor for Gas Detection", *Proceedings Transducers'01*, ISBN 3-540-42150-5, 2001, pp 806–809.
21. M. H. Westbrook, J. D. Turner: " *Automotive Sensors*"; Institute of Physics Publishing, Bristol and Philadelphia; (1994) ; ISBN 0-7503-0293-3.
22. B. W. van Odheusden: " Silicon Thermal Flow Sensors". *Sensors & Actuators* **A30**: 5–26, 1992.
23. L. Qiu, E. Obermeier, A. Schubert: " A Microsensor with Integrated Heat Sink and Flow Guide for Gas Flow Sensing Applications"; *Transducers '95*;Stockholm, Sweden, pp 520–523, 1995.

24. H. E. de Bree, et al. The μ-Flown, a Novel Device Measuring Acoustical Flows"; *Transducers '95*,Stockholm, Sweden, pp. 552–557, 1995.
25. U. Dillinger, et al. Low Power Consumption Thermal Gas Flow Sensor Based on Thermopiles of Highly Effective Thermoelectric Materials"; *Proc. Eurosensors X*,Belgium, September 8–11, 1997, pp. 449–452.
26. http://cms.hlplanar.de/index.php.
27. http://rb-k.bosch.de/de/start/product_ds_06_luftms_sens.html.
28. http://www.umweltsensortechnik.de/index3.htm.
29. http://www.figarosensor.com/.
30. G. Sberveglieri, et al. A new technique for growing large surface area SnO_2 thin films (R. G. T. O. Technique), *Semicond. Sci. Technol.*, **5**: 1231–1233, 1990.
31. S. Semancik, R. E. Cavicchi, K. G. Kreider, J. S. Suehle, P. Chaparla," Selected area deposition of multiple active films for conductometric microsensor arrays", *Proc. Transducers '95, EUROSENSORS IX*, (1995), Stockholm, Sweden, p. 831–834.
32. F. DiMeo, Jr., *et al.*" Heteroepitaxy of conducting oxides on silicon using oxide buffer layers", *Proc. 6th Int. Meet. Chem. Sensors*,July 22–25, 1996.
33. Comini, E.; Faglia, G.; Sberveglieri, G., *et al. Appl. Phys. Lett.* **81**, 2002, 1869.
34. M. Epifani, L. Francioso, P. Siciliano, A. Helwig, G. Mueller, R. Díaz, J. Arbiol, J. R. Morante: " SnO_2 thin films from metalorganic precursors: Synthesis, characterization, microelectronic processing, and gas-sensing properties"; *Proc. EMRS 2006*,29 May–2 July 2006Nizza; Sensors & Actuators B (2007, in press)
35. U. Hoefer, *et al.*" CO and NO_2 thin-film SnO_2 gas sensors on Si substrates", *Sensors and Actuators*, **B22**: 115–119, 1994.
36. H.-E. Endres, *et al.*:" A thin-film SnO_2 sensor system for simultaneous detection of CO and NO_2 with neural signal evaluation", *Proc. 6th Int. Meeting Chem. Sensors*,July 22–25, 1996. Gaithersburg, MD.
37. W. Hellmich, G. Müller, T. Doll, I. Eisele: " Field-Effect-Induced Gas Sensitivity Changes in Metal Oxides"; *Sensors & Actuators* **B43** (1997) 132–139.
38. EU-funded project, "GOODFOOD" (2006).
39. A. Helwig, O. Schulz, I. Sayhan, G. Müller: " Multi-criteria Fire Detectors for Aeronautic Applications"; *Proc. TRANSFAC 2006*, San Sebastian, Spain, September 2006.
40. O. Schulz, G. Müller, M. Lloyd, A. Ferber: " The Impact of Environmental Parameters on the Emission from Micromachined IR Sources", *Sensors & Actuators* **A121** (2005) 172–180.
41. J. Spannhake, O. Schulz, A. Helwig, G. Müller, Th. Doll: " Design, development and operational concept of an advanced MEMS IR source for miniaturized gas sensor systems", *Proc. IEEE Sensors 2005*, Irvine, CA, USA, Oct 31–Nov 3, 2005.
42. J. Spannhake, O. Schulz, A. Helwig, A. Krenkow, G. Müller, Th. Doll:"High-Temperature MEMS Heater Platforms: Long-term performance of metal and semiconductor heater materials", ISSN 1424-8220© 2005 by MDPI, http://www.mdpi.net/sensors.
43. K. Schjølberg-Henriksen, A. Ferber, O. Schulz, S. Moe, D. T. Wang, M. Lloyd, W. Legner, K.-H. Suphan, R. W. Bernstein, H. Rogne, G. Müller: " Sensitive and selective photo acoustic gas sensor suitable for high-volume manufacturing", *Proceedings of IEEE Sensors Conference*, Daegu, Korea, October 22–25, 2006.
44. J. Spannhake, A. Helwig, G. Müller, G. Sberveglieri, G. Faglia, T. Wassner, M. Eickhoff: " SnO_2:Sb—A new material for high-temperature MEMS heater applications—performance and limitations"; *Sensors & Actuators*(2007 in press)
45. R. W. Bickes, Jr. and A. C. Schwarz,Semiconductor Bridge (SCB), Ignitor,U.S. Patent No. 4,708,060.
46. http://www.cismst.de/deutsch/datenblaetter/ai-silanz.pdf.

JAN SPANNHAKE
ANDREAS HELWIG
ALOIS FRIEDBERGER
GERHARD MÜLLER
EADS Corporate Research Centre Germany

WOLFGANG HELLMICH
European Patent Attorney